PROCEEDINGS OF SCIENCE

Nucleon axial, tensor, and scalar charges and σ-terms in lattice QCD

Constantia Alexandrou,[a,b] **Simone Bacchio,**[b] **Jacob Finkenrath,**[c] **Christos Iona,**[a,*] **Giannis Koutsou,**[b] **Yan Li**[a] **and Gregoris Spanoudes**[a]

[a] *Department of Physics, University of Cyprus, P.O. Box 20537, 1678 Nicosia, Cyprus*

[b] *Computation-based Science and Technology Research Center, The Cyprus Institute, 20 Kavafi Str., Nicosia 2121, Cyprus*

[c] *Department of Theoretical Physics, European Organization for Nuclear Research, CERN, CH-1211 Geneva 23, Switzerland*

E-mail: iona.n.christos@ucy.ac.cy

We determine the nucleon axial, scalar and tensor charges at the continuum limit by analyzing three $N_f = 2+1+1$ twisted mass fermion ensembles with all quark masses tuned to approximately their physical values. We include all contributions from valence and sea quarks. We use the Akaike Information Criterion to evaluate systematic errors due to excited states and the continuum extrapolation. For the nucleon isovector axial charge we find $g_A^{u-d} = 1.250(24)$, in agreement with the experimental value. We compute the axial, tensor and scalar charges for each quark flavor. The axial charge provides crucial information on the intrinsic spin carried by quark in the nucleon and the the latter two provide input for experimental searches of physics beyond the standard model. Moreover, we extract the nucleon σ-terms and find $\sigma_{\pi N} = 41.9(8.1)$ MeV, for the strange $\sigma_s = 30(17)$ MeV and for the charm $\sigma_c = 82(29)$ MeV. We also present preliminary results on the isovector quantities using a fourth ensemble at smaller lattice spacing.

The 41st International Symposium on Lattice Field Theory (LATTICE2024)
28 July - 3 August 2024
Liverpool, UK

*Speaker

PoS(LATTICE2024)316

1. Introduction

The nucleon axial, tensor, and scalar charges, along with the σ-terms, are fundamental quantities that provide insights into nucleon structure. The axial charge, g_A^{u-d}, governs neutron beta decay and plays a critical role in neutrinoless double-beta decay and tests of CKM matrix unitarity. Flavor-diagonal axial charges, g_A^f, describe the intrinsic spin, $\frac{1}{2}\Delta\Sigma_q$, carried by quarks in the nucleon, as measured in deep inelastic scattering at facilities, such as Jefferson Lab and CERN, and also targeted at the future Electron-Ion Collider (EIC).

The isovector tensor and scalar charges, g_T^{u-d} and g_S^{u-d}, are crucial for constraining beyond the Standard Model (BSM) interactions to be searched in experiments like DUNE [1], COHERENT [2], GEMMA [3], and dark matter detection searches [4–6]. Accurate determination of the tensor charge is key to understanding the transversity parton distribution function, while the nucleon σ-terms quantify quark mass contributions to the nucleon mass.

We compute the nucleon charges and σ-terms using twisted mass fermion ensembles at three lattice spacings and present preliminary results for the isovector charges at a fourth, finer lattice spacing. These $N_f = 2 + 1 + 1$ ensembles, simulated by the Extended Twisted Mass Collaboration (ETMC), use quarks fixed near their physical masses [7], allowing precise determinations without chiral extrapolations.

2. Nucleon Matrix Elements

The nucleon axial, tensor, and scalar charges for each quark flavor f, denoted as $g^f_{\mathrm{A,T,S}}$, are extracted from the matrix elements of the corresponding axial, tensor, and scalar operators at zero momentum transfer:

$$\langle N|\bar{\psi}^f \Gamma_{\mathrm{A,S,T}} \psi^f |N\rangle = g^f_{\mathrm{A,T,S}} \bar{u}_N \Gamma_{\mathrm{A,S,T}} u_N \,, \tag{1}$$

where u_N is the nucleon spinor, and the operator structures are $\Gamma_A = \gamma_\mu\gamma_5$ (axial-vector), $\Gamma_S = \mathbb{1}$ (scalar), and $\Gamma_T = \sigma_{\mu\nu}$ (tensor), with $\sigma_{\mu\nu} = \frac{i}{2}[\gamma_\mu, \gamma_\nu]$. The renormalization group invariant σ^f-term is given by $\sigma^f = m_f \langle N|\bar{\psi}^f\psi^f|N\rangle$, with m_f the mass of the quark with flavor f.

Table 1: Parameters of the $N_f = 2 + 1 + 1$ ensembles analyzed in this work. In the first column, we give the name of the ensemble, in the second the abbreviated name, in the third the lattice volume, in the fourth $\beta = 6/g^2$ with g the bare coupling constant, in the fifth the lattice spacing and in the sixth the pion mass. Lattice spacings and pion masses for B64, C80 and D96 are taken from Ref. [8] and for E112 from Ref. [9]. In the last column we list the number of configurations used per ensemble.

Ensemble	Abrv.	V/a^4	β	$a\ [fm]$	$m_\pi\ [MeV]$	Config.
cB211.072.64	B64	$64^3 \times 128$	1.778	0.07957(13)	140.2(2)	749
cC211.060.80	C80	$80^3 \times 160$	1.836	0.06821(13)	136.7(2)	400
cD211.054.96	D96	$96^3 \times 192$	1.900	0.05692(12)	140.8(2)	494
cE211.044.112	E112	$112^3 \times 224$	1.960	0.04892(11)	136.5(2)	258[1]

The twisted-mass fermion discretization provides automatic $O(a)$ improvement [10, 11]. A clover term [12] is included to reduce isospin-breaking effects. The parameters of the ensembles

[1] This ensemble is currently under production and in this proceeding we show preliminary results for a subset of the configurations planned.

used in this study are listed in Table 1. Lattice spacings and pion masses for the B64, C80 and D96 are taken from Ref. [8] determined within the meson sector. These values agree with those determined from the nucleon mass [13]. The lattice spacing and pion mass for the E112 ensemble are taken from Ref. [9].

Nucleon charges are extracted by combining two- and three-point nucleon correlation functions. To ensure consistent errors, statistics for three-point functions are increased as the source-sink time separation is increased to keep the error approximately constant. The spectral decompositions of the two- and three-point functions are:

$$C(\Gamma_0, \vec{p}; t_s) = \sum_{i}^{\infty} c_i(\vec{p}) e^{-E_i(\vec{p})t_s}, \tag{2}$$

$$C^{\mu}(\Gamma_k, \vec{q}; t_s, t_{ins}) = \sum_{i,j}^{\infty} A_{\mu}^{i,j}(\Gamma_k, \vec{q}) e^{-E_i(\vec{0})(t_s - t_{ins}) - E_j(\vec{q})t_{ins}}, \tag{3}$$

where t_s is the source-sink time separation and $t_{\rm ins}$ the time separation between current insertion and source and $\vec{p}$ and $\vec{q}$ are the two-point function sink momentum and three-point function momentum transfer respectively. The axial case, for example, is given as the ratio of the axial current three- to two-point function for $\vec{p} = \vec{q} = 0$:

$$R_{\mu}^{A}(t_s, t_{ins}) = \frac{C_{\mu}^{3pt}(\Gamma_k; t_s, t_{ins})}{C^{2pt}(t_s)} \xrightarrow[t_{ins}\to\infty]{t_s - t_{ins}\to\infty} g_A. \tag{4}$$

In the large time separation limit, the ratio converges to the corresponding charge, e.g., g_A. We analyze excited state contributions by performing two-state fits, where we explore a wide parameter space and average results using the Akaike Information Criterion (AIC) [14, 15]. The calculated nucleon matrix elements have been renormalized nonperturbatively by employing the RI′/MOM scheme followed by perturbative conversion to the $\overline{\rm MS}$ scheme at the reference scale of 2 GeV (see Ref. [16] for more details).

3. Results

In Fig. 1 we present an example of a two-state fit analysis for the nucleon isovector axial charge g_A^{u-d}. The isovector axial-vector operator is given by:

$$O_A^{u-d} \equiv A_{\mu} = \bar{u}\gamma_{\mu}\gamma_5 u - \bar{d}\gamma_{\mu}\gamma_5 d, \tag{5}$$

where u and d are the up and down quark fields, respectively. For the axial case, due to chiral perturbation theory arguments [17, 18], to better estimate the isovector axial charge, we include in the fit the three-point function of the temporal component of the axial-vector current with one unit of momentum transfer, $C^0(\Gamma_k, \frac{2\pi}{L}\hat{k}; t_s, t_{ins})$ together with the corresponding two-point function, to help extract the excited state energies $E_i(\vec{q})$, where L is the spatial length of the lattice and $\hat{k}$ a unit vector in the k spatial direction.

In our fitting procedure, we vary the smallest value of the sink time t_s we use for the fitting of the ratio, $t_s^{\rm low}$, as well as the lowest time slice in the fitting of the two-point functions, t_{2pt}^{low}. We also vary the number of insertion time slices that we keep in the fits. We use $t_{ins} \in [t_{ins,0}, t_s - t_{ins,s}]$.

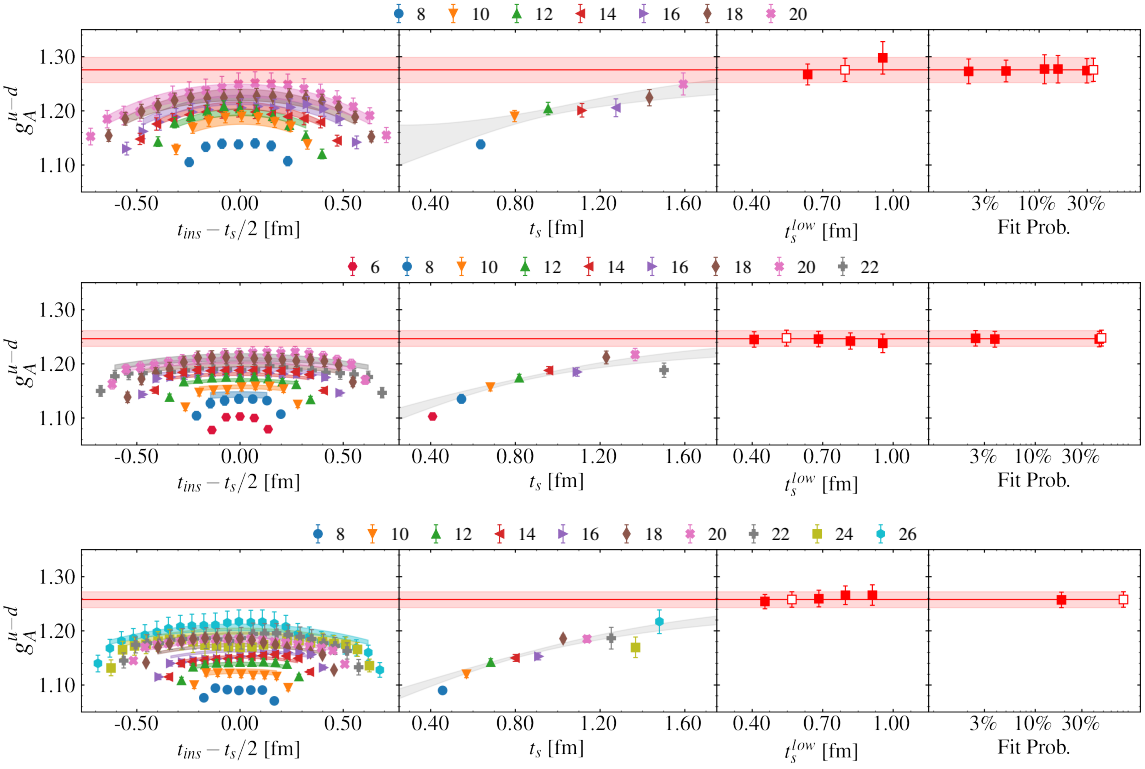

Figure 1: We present the ratio and fit results for all ensembles, for the isovector axial charge. In the legend, we give the symbols used to denote the various values of t_s/a. The top row shows the analysis for g_A^{u-d} for the B64 ensemble, the middle row for C80 and the bottom for D96. The first column shows results on the ratio versus $t_{ins} - t_s/2$. The horizontal bands are the model averaged values. In the second column, we show the ratio versus t_s for $t_{ins} = t_s/2$. The gray band is the result of the two-state fit model with the highest probability. In the third column, we show the extracted values as a function of the lowest value of t_s included in the fits, where we give the results for the most probable model for a given value of t_s^{low}. In the last column, we present the weights for fit models whose probabilities exceed 1%. The open symbols are the most probable models taking into account fits using all t_s^{low}.

For the charges we work at $Q^2 = 0$ so we fix $t_{ins,0} = t_{ins,s}$, removing an equal number of time slices on the source and the sink sides. The extracted values show almost no dependence on on t_s^{low}. The results in the third column of Fig. 1 represent the highest probability model for each t_s^{low}, varying $t_{\text{ins},0}$ and $t_{2\text{pt}}^{\text{low}}$.

To extrapolate to the continuum limit ($a \to 0$), we use the results from the ensembles B64, C80 and D96. We carry out three types of extrapolation and evaluate a combined systematic and statistical error via a model average over the three fits. Namely, we use a linear fit in a^2 and a constant fit either using all three ensembles or when omitting the coarser ensemble, B64. A strong dependence on the lattice spacing will result in a model average favoring the linear fit, while a mild a^2 dependence will lead to a model average favoring the two constant fits. The continuum limit extrapolation for the isovector axial charge is shown in Fig. 2, along with the weights for each type of extrapolation. In Table 2 we present our continuum limit results for the axial, scalar and tensor 2-, 3- and 4- flavor isovector and isoscalar combinations, as well as the single flavor charges for each case. All results per ensemble and after continuum extrapolation can be found in Ref. [16].

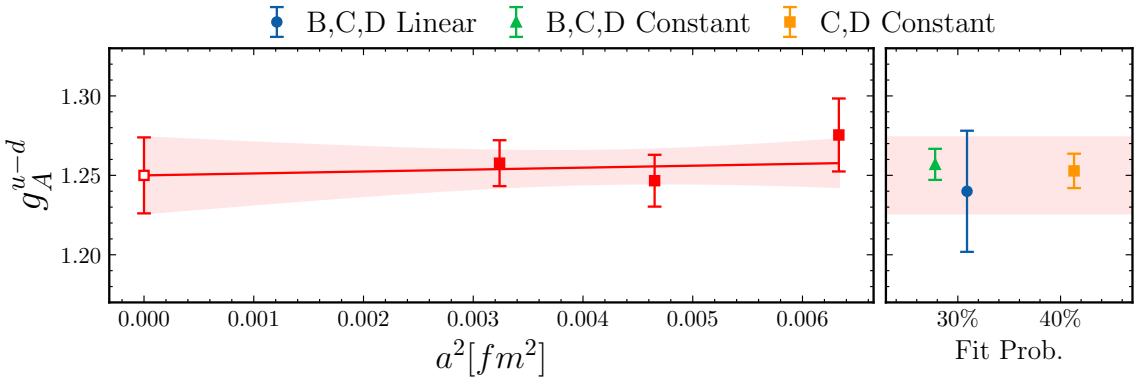

Figure 2: In the left panel, we show the continuum limit of the nucleon isovector axial charge (open symbol and band) extrapolated using the B64, C80 and D96 ensembles (filled symbols). The extrapolation is the result of a model average, which combines linear and constant fits as explained in the text. In the right panel, we show the weights for each type of fit, namely the linear extrapolation is represented by a blue circle, the constant extrapolation including all three ensembles by a green triangle and the constant extrapolation using the C90 and D96 ensembles by an orange square. The red band is the model average value from the three fits.

Table 2: Values for the 2-, 3-, and 4-flavor isovector and isoscalar combinations (top) and the extracted single flavor charges (bottom) in the continuum limit, using the model average strategy described in the text.

	$u-d$	$u+d$	$u+d-2s$	$u+d+s-3c$	$u+d+s+c$
g_A	1.250(24)	0.423(33)	0.490(20)	0.343(55)	0.382(70)
g_S	1.08(31)	11.5(2.2)	11.2(2.1)	11.4(2.1)	12.2(2.2)
g_T	0.955(29)	0.561(34)	0.561(33)	0.569(37)	0.557(34)

	u	d	s	c
g_A	0.832(28)	-0.417(22)	-0.037(18)	0.003(13)
g_S	6.4(1.1)	5.30(98)	0.16(37)	0.09(26)
g_T	0.756(29)	-0.196(12)	-0.0009(11)	-0.0028(26)

In this work, we also calculated the nucleon σ-terms, which are defined as

$$\sigma^f = m_f \langle N|\bar{\psi}_f \psi_f|N\rangle \ , \quad \sigma^{u+d} = m_{ud} \langle N|\bar{u}u + \bar{d}d|N\rangle \, , \tag{6}$$

where m_f is the quark mass for a given flavor f, m_{ud} is the average light quark mass, and $|N\rangle$ is the nucleon state. The value of σ^{u+d}, also referred to as $\sigma^{\pi N}$, is determined from phenomenological analyses using experimental inputs. These quantities are fundamental in QCD, providing insights into the quark content of the nucleon and serving as a measure of chiral symmetry breaking.

The nucleon σ-terms are extracted from the scalar matrix elements, including disconnected quark loops. The twisted mass formulation simplifies renormalization compared to standard Wilson fermions, as it eliminates additive mass renormalization and ensures that the multiplicative renormalization of the scalar current and quark mass cancel. Our results for $\sigma^{\pi N}$, σ^s, and σ^c are presented in Table 3.

In Fig. 3, we compare our results for the isovector charges with recent results from other lattice QCD studies, as well as with previous analyses of these quantities by ETMC. The results presented in this work are the only ones obtained by taking the continuum limit using ensembles simulated

Table 3: Results for the nucleon σ-terms (in MeV) in the continuum limit. For $\sigma_{\pi N}$ and for σ_s we follow the same extrapolation procedure as described in Fig. 2, while for σ_c we use a single constant extrapolation.

$\sigma^{\pi N}$	41.9(8.1)	σ^s	30(17)	σ^c	82(29)

directly at the physical pion mass. In contrast, all other collaborations use ensembles with pion masses heavier than physical or combine one or two physical point ensembles with heavier-than-physical ones. Since results at the physical point typically have larger statistical uncertainties, their extrapolations may be more influenced by the heavier-than-physical ensemble data.

We observe very good agreement among lattice QCD results by different collaborations for all isovector charges. Moreover, our value for the isovector axial charge g_A^{u-d}, is compatible with the experimental value [19].

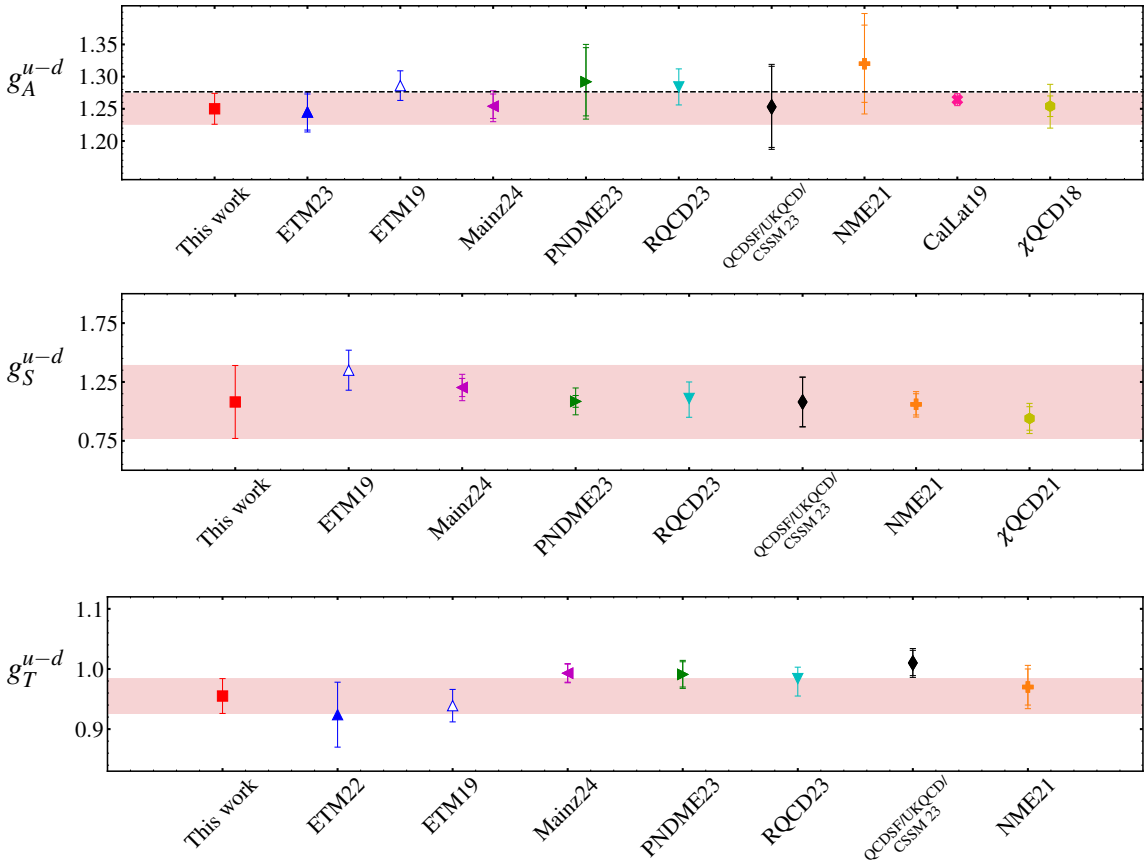

Figure 3: Comparison of the results of this work with other lattice QCD results, for the isovector axial, scalar and tensor charges. Our results are shown with the red square and red error band. The blue triangles show previous ETMC results, for g_A^{u-d} [20] and for g_T^{u-d} [21], while Ref. [22] gives results on all three isovector charges including g_s^{u-d} for the B64 ensemble. Open symbols represent results without a continuum limit extrapolation. The magenta triangles show recent results from the Mainz group [23], the green triangles from PNDME [24], the cyan triangles from RQCD [25], the black diamonds from the QCDSF/UKQCD/CSSM collaboration [26], the orange crosses from NME [27], the pink cross from CalLat [28] and the yellow hexagons from χQCD [29, 30]. For g_A^{u-d}, the dashed line represents the experimental value [19].

3.1 Preliminary results using the E112 ensemble with $a \approx 0.05$ fm.

In this section, we present preliminary results for our new physical point ensemble, simulated at a finer lattice spacing ($a \approx 0.05$ fm), that will aid in the continuum limit extrapolation of all quantities. The details of the ensemble are listed in Table 1.

In Fig. 4, we show the ratios and preliminary fits for the isovector axial, scalar and tensor charges for the E112 ensemble. We observe a good signal to noise ratio for the analyzed configurations. We aim to use more than 500 configurations, increase statistics and the value of t_s. Moreover, we will calculate the disconnected contributions and perform the continuum limit extrapolation using all four ensembles.

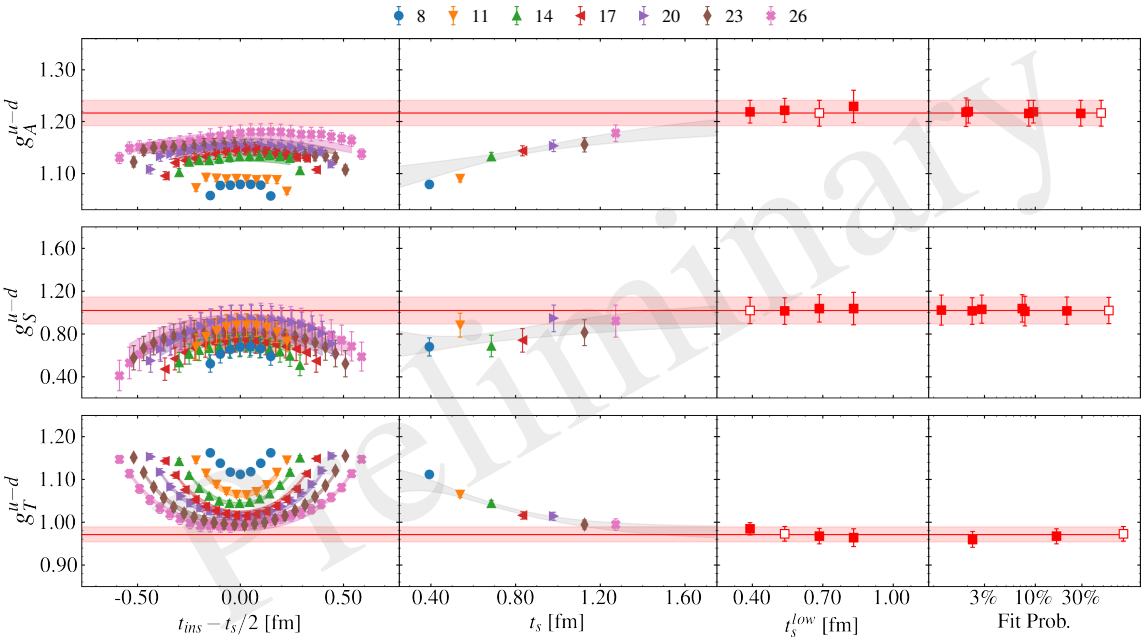

Figure 4: Ratio and preliminary fit results for the currently available data of the E112 ensemble, for the isovector charges. The notation is the same as in Fig. 1.

4. Conclusions

We present results on the nucleon axial, scalar and tensor charges, as well as on the nucleon σ-terms, using three $N_f = 2+1+1$ twisted mass clover-improved fermions ensembles, with quark masses tuned to reproduce their physical values. This enables us, for the first time, to determine these charges and σ-terms at the continuum limit using only physical point ensembles, avoiding any chiral extrapolations. Our future goal is to include the fourth ensemble with a finer lattice spacing of $a \approx 0.05$ fm for which we include preliminary results in this proceeding. This finer ensemble will further refine our continuum limit extrapolations and increase the accuracy of our final values.

Acknowledgments

We thank the ETM collaboration for their support and particularly acknowledge Matteo Di Carlo, Antonio Evangelista, Roberto Frezzotti, Giuseppe Gagliardi, and Vittorio Lubicz for discussions and crosschecks on renormalization factors. We are also grateful to Georg Bergner, Petros Dimopoulos, Bartosz Kostrzewa, and Urs Wenger for their contributions to the $N_f = 4$ gauge ensembles.

C.A. and G.K. acknowledge partial support from the European Joint Doctorate AQTIVATE (Grant Agreement No. 101072344). Y.L. and Ch.I. are supported by the Excellence Hub project "3D-nucleon" (id EXCELLENCE/0421/0043) co-financed by the European Regional Development Fund and the Republic of Cyprus through the Research and Innovation Foundation and by the University of Cyprus projects "Nucleon-GPDs" and "PDFs-LQCD". S.B. and G.K. acknowledge support from the Excellence Hub project "NiceQuarks" (id EXCELLENCE/0421/0195). S.B. and J.F. are supported by the Inno4scale project, which received funding from the European High-Performance Computing Joint Undertaking (JU) under Grant Agreement No. 101118139. J.F. also acknowledges support from the DFG research unit FOR5269 "Future methods for studying confined gluons in QCD" and the Next Generation Triggers project (https://nextgentriggers.web.cern.ch).

We thank the Gauss Centre for Supercomputing e.V. (www.gauss-centre.eu) for access to SuperMUC-NG at the Leibniz Supercomputing Centre, JUWELS [31] and JUWELS Booster [32] at the Jülich Supercomputing Centre (JSC). Results were partially created within the JUWELS Booster EA program with assistance from the JUWELS Booster Project Team (JSC, Atos, ParTec, NVIDIA). We acknowledge the Swiss National Supercomputing Centre (CSCS) and the EuroHPC Joint Undertaking for awarding access to the LUMI supercomputer, owned by the EuroHPC Joint Undertaking, hosted by CSC (Finland) and the LUMI consortium, through the Chronos programme under project IDs CH16-CYP. We are grateful to CINECA and the EuroHPC JU for awarding access to supercomputing facilities hosted at CINECA and to Leonardo-Booster through the Extreme Scale Access Call grant EHPC-EXT-2024E01-027. Finally, we acknowledge computing time on Cyclone at the Cyprus Institute (project IDs P061, P146, and pro22a10951).

References

[1] I. Bischer and W. Rodejohann, *General Neutrino Interactions at the DUNE Near Detector*, *Phys. Rev. D* **99** (2019) 036006 [1810.02220].

[2] COHERENT collaboration, *Observation of Coherent Elastic Neutrino-Nucleus Scattering*, *Science* **357** (2017) 1123 [1708.01294].

[3] A. Beda, V. Brudanin, V. Egorov, D. Medvedev, V. Pogosov, M. Shirchenko et al., *The results of search for the neutrino magnetic moment in GEMMA experiment*, *Adv. High Energy Phys.* **2012** (2012) 350150.

[4] T. Marrodán Undagoitia and L. Rauch, *Dark matter direct-detection experiments*, *J. Phys. G* **43** (2016) 013001 [1509.08767].

[5] M.V. Chizhov, *Search for tensor interactions in kaon decays at DAPHNE*, *Phys. Lett. B* **381** (1996) 359 [hep-ph/9511287].

[6] L. Dhargyal, *New tensor interaction as the source of the observed CP asymmetry in* $\tau \to K_S \pi \nu_\tau$, *Springer Proc. Phys.* **203** (2018) 329 [1610.06293].

[7] C. Alexandrou et al., *Simulating twisted mass fermions at physical light, strange and charm quark masses*, *Phys. Rev.* **D98** (2018) 054518 [1807.00495].

[8] Extended Twisted Mass collaboration, *Lattice calculation of the short and intermediate time-distance hadronic vacuum polarization contributions to the muon magnetic moment using twisted-mass fermions*, *Phys. Rev. D* **107** (2023) 074506 [2206.15084].

[9] Extended Twisted Mass Collaboration (ETMC) collaboration, *Strange and charm quark contributions to the muon anomalous magnetic moment in lattice QCD with twisted-mass fermions*, 2411.08852.

[10] Alpha collaboration, *Lattice QCD with a chirally twisted mass term*, *JHEP* **08** (2001) 058 [hep-lat/0101001].

[11] R. Frezzotti and G.C. Rossi, *Chirally improving Wilson fermions. 1. O(a) improvement*, *JHEP* **08** (2004) 007 [hep-lat/0306014].

[12] B. Sheikholeslami and R. Wohlert, *Improved Continuum Limit Lattice Action for QCD with Wilson Fermions*, *Nucl. Phys.* **B259** (1985) 572.

[13] Extended Twisted Mass collaboration, *Quark masses using twisted-mass fermion gauge ensembles*, *Phys. Rev. D* **104** (2021) 074515 [2104.13408].

[14] W.I. Jay and E.T. Neil, *Bayesian model averaging for analysis of lattice field theory results*, *Phys. Rev. D* **103** (2021) 114502 [2008.01069].

[15] E.T. Neil and J.W. Sitison, *Improved information criteria for Bayesian model averaging in lattice field theory*, *Phys. Rev. D* **109** (2024) 014510 [2208.14983].

[16] C. Alexandrou, S. Bacchio, J. Finkenrath, C. Iona, G. Koutsou, Y. Li et al., *Nucleon charges and σ-terms in lattice QCD*, 2412.01535.

[17] O. Bär, *$N\pi$-state contamination in lattice calculations of the nucleon axial form factors*, *Phys. Rev. D* **99** (2019) 054506 [1812.09191].

[18] O. Bär, *Nucleon-pion-state contribution in lattice calculations of the nucleon charges g_A, g_T and g_S*, *Phys. Rev. D* **94** (2016) 054505 [1606.09385].

[19] B. Märkisch et al., *Measurement of the Weak Axial-Vector Coupling Constant in the Decay of Free Neutrons Using a Pulsed Cold Neutron Beam*, *Phys. Rev. Lett.* **122** (2019) 242501 [1812.04666].

[20] Extended Twisted Mass collaboration, *Nucleon axial and pseudoscalar form factors using twisted-mass fermion ensembles at the physical point*, *Phys. Rev. D* **109** (2024) 034503 [2309.05774].

[21] C. Alexandrou et al., *Moments of the nucleon transverse quark spin densities using lattice QCD*, *Phys. Rev. D* **107** (2023) 054504 [2202.09871].

[22] C. Alexandrou, S. Bacchio, M. Constantinou, J. Finkenrath, K. Hadjiyiannakou, K. Jansen et al., *Nucleon axial, tensor, and scalar charges and σ-terms in lattice QCD*, *Phys. Rev. D* **102** (2020) 054517 [1909.00485].

[23] D. Djukanovic, G. von Hippel, H.B. Meyer, K. Ottnad and H. Wittig, *Improved analysis of isovector nucleon matrix elements with Nf=2+1 flavors of O(a) improved Wilson fermions*, *Phys. Rev. D* **109** (2024) 074507 [2402.03024].

[24] Precision Neutron Decay Matrix Elements (PNDME) collaboration, *Nucleon isovector axial form factors*, *Phys. Rev. D* **109** (2024) 014503 [2305.11330].

[25] RQCD collaboration, *Octet baryon isovector charges from Nf=2+1 lattice QCD*, *Phys. Rev. D* **108** (2023) 034512 [2305.04717].

[26] QCDSF/UKQCD/CSSM collaboration, *Constraining beyond the standard model nucleon isovector charges*, *Phys. Rev. D* **108** (2023) 094511 [2304.02866].

[27] Nucleon Matrix Elements (NME) collaboration, *Precision nucleon charges and form factors using (2+1)-flavor lattice QCD*, *Phys. Rev. D* **105** (2022) 054505 [2103.05599].

[28] A. Walker-Loud et al., *Lattice QCD Determination of g_A*, *PoS* **CD2018** (2020) 020 [1912.08321].

[29] J. Liang, Y.-B. Yang, T. Draper, M. Gong and K.-F. Liu, *Quark spins and Anomalous Ward Identity*, *Phys. Rev. D* **98** (2018) 074505 [1806.08366].

[30] χQCD collaboration, *Nucleon isovector scalar charge from overlap fermions*, *Phys. Rev. D* **104** (2021) 094503 [2103.12933].

[31] Jülich Supercomputing Centre, *JUWELS: Modular Tier-0/1 Supercomputer at the Jülich Supercomputing Centre*, *Journal of large-scale research facilities* **5** (2019) A135.

[32] Jülich Supercomputing Centre, *JUWELS Cluster and Booster: Exascale Pathfinder with Modular Supercomputing Architecture at Juelich Supercomputing Centre*, *Journal of large-scale research facilities* **7** (2021) A183.